applied sciences

MDPI

Communication

Novel Pr-Doped $BaLaInO_4$ Ceramic Material with Layered Structure for Proton-Conducting Electrochemical Devices

Nataliia Tarasova [1,2,*], Anzhelika Bedarkova [1,2] and Irina Animitsa [1,2]

[1] The Institute of High Temperature Electrochemistry of the Ural Branch of the Russian Academy of Sciences, Yekaterinburg 620000, Russia
[2] Institute of Hydrogen Energy, Ural Federal University, Yekaterinburg 620000, Russia
* Correspondence: natalia.tarasova@urfu.ru

Abstract: One of the urgent tasks of applied materials science is the creation of novel high-effective materials with target properties. In the area of energy systems, there is a problem in the conversion of chemical energy to electricity without mechanical work. Hydrogen energy provides a way using electrochemical devices such as protonic ceramic fuel cells. Novel advanced proton-conducting materials with the top characteristics of target properties are strictly needed. Layered perovskites are a novel and promising class of protonic conductors. In this work, the layered perovskite $BaLa_{0.9}Pr_{0.1}InO_4$ was obtained and investigated as a protonic conductor for the first time. The possibility for water intercalation and proton transport is proved. It was shown that isovalent doping $Pr^{3+} \rightarrow La^{3+}$ leads to an increase in the crystal lattice size, proton concentration and proton mobility. The proton conductivity value for doped $BaLa_{0.9}Pr_{0.1}InO_4$ composition is 18 times greater than for undoped $BaLaInO_4$ composition. Layered perovskites based on $BaLaInO_4$ are promising materials for application in proton-conducting electrochemical devices.

Keywords: layered perovskite; oxygen-ion conductivity; proton conductivity; hydrogen energy; Ruddlesden–Popper structure

check for updates

Citation: Tarasova, N.; Bedarkova, A.; Animitsa, I. Novel Pr-Doped $BaLaInO_4$ Ceramic Material with Layered Structure for Proton-Conducting Electrochemical Devices. *Appl. Sci.* **2023**, *13*, 1328. https://doi.org/10.3390/app13031328

Academic Editors: Luis Hernández-Callejo, Jesús Armando Aguilar Jiménez and Carlos Meza Benavides

Received: 13 December 2022
Revised: 17 January 2023
Accepted: 17 January 2023
Published: 19 January 2023

1. Introduction

Applied materials science plays an important role in the development of various areas of human life. Critical areas such as medicine, energy and mechanical engineering cannot develop without the creation of new materials with targeted properties. Ceramic materials are required for very different needs such as medical applications (endoprosthetics) [1–6] and components for various electrochemical devices [7–12], as examples. The high priority of sustainable development necessitates the development of advanced energy technologies, one of them being hydrogen energy [13–16]. The switchover to renewable energy is, actually, not only for increasing energetically efficiency, but, also, due to the pursuit in decreasing climate changes and the lowering of cases of respiratory diseases [17–23]. Hydrogen energy is considered as an actual, sustainable and promising approach for energy generation [24–35]. This industry includes aspects such as the production, transportation and use of hydrogen as an energy source. The conversion of the chemical energy of hydrogen oxidation to electrical energy can be implemented using electrochemical devices such as protonic ceramic fuel cells [36–41]. This requires new high-effective materials such as electrodes, electrolytes and interconnectors with good compatibility between each other. The traditional and most investigated proton-conducting materials are barium cerate zirconates $BaCeO_3$-$BaZrO_3$, which are characterized by perovskite structure [42,43]. However, they are characterized by a relatively low concentration of protons and low chemical resistance to carbon dioxide. Consequently, novel advanced proton-conducting materials with top characteristics of target properties are strictly needed.

Layered perovskite structure is related to classical perovskite structure. The main difference is the separation of the perovskite framework by the layers with different structures.

Layered perovskites with the general formula $AA'_nB_nO_{3n+1}$ belong to members of layered perovskite family such as compositions with the Ruddlesden–Popper structure. Perovskite slabs $A'BO_3$ are divided by the rock salt layers AO in this structural type, and the existence of compositions with a different "n" is possible. Layered structures provide a concentration of protons an order of magnitude higher than that of classic perovskites. The realization of proton transport was proved for monolayer perovskites such as $BaNdInO_4$ [44–48], $BaNdScO_4$ [49], $SrLaInO_4$ [50–54], $BaLaInO_4$ [55–60] and compositions based on them in the last few years [61]. Such compositions can be potentially used as electrolytic materials in the proton-conducting fuel cells. Various types of doping, including cationic [62] and oxyanionic [63], were investigated. However, the substitutions were implemented by the ions with a stable oxidation state. Meanwhile, the introduction of ions capable of changing their valence can provide control over the contributions of the electronic and ionic components of conductivity. In the future, this can ensure the creation of electrode and electrolyte materials with the same crystal structure and similar chemical composition, which should provide excellent compatibility. In this work, a Pr-doped ceramic material based on $BaLaInO_4$ was obtained and investigated for the first time. The possibility of protonic transport was revealed.

2. Experimental Procedure

The phase $BaLa_{0.9}Pr_{0.1}InO_4$ was synthesized via the nitrate–citrate route according to [52]. The starting reagents $Ba(NO_3)_2$, $In(NO_3)_3{\cdot}6H_2O$, $Pr(NO_3)_3{\cdot}6H_2O$ and $La(NO_3)_3{\cdot}9H_2O$ were used. The X-ray diffraction analysis (XRD) was implemented at the Cu K_α diffractometer Bruker Advance D8. The full profile Le Bail regiments were implemented via the FullProf Suite software. The method of scanning electron microscopy (SEM) of powder and ceramic samples was realized using microscope VEGA3 TESCAN coupled with an energy-dispersive X-ray spectroscopy system (EDS).

The thermogravimetry (TG) measurements were implemented by the Netzsch Analyser STA 409 PC. The samples were initially hydrated using the method of cooling from 1000 to 150 °C (0.5 °C/min) at wet Ar flow. During TG-measurements, the samples were heated from 40 to 1000 °C with the speed 10 °C/min at dry Ar flow.

The resistance of ceramic samples was collected via the impedance spectrometer Elins Z-1000P. The ceramic pellets with a 10 mm diameter and 2 mm thickness were pressed for the investigations. Pt-electrodes were applied on the surfaces of the samples. The temperature range 200–1000 °C was covered, and the speed of cooling was 1°/min. The dry atmosphere was obtained by the circulating of air or Ar through phosphorus pentoxide ($pH_2O = 3.5 \times 10^{-5}$ atm). The wet atmosphere was obtained by the passing of air or Ar through a saturated solution of potassium bromide ($pH_2O = 2 \times 10^{-2}$ atm).

3. Results and Discussions

The phase characterization of composition $BaLa_{0.9}Pr_{0.1}InO_4$ was made using XRD analysis. Figure 1a represents the Le Bail refinement of the X-ray obtained data. The composition is single phase and it has orthorhombic symmetry (*Pbca* space group). The image of the crystal structure of the monolayer perovskite is presented in the inset of Figure 1a. The introduction of Pr^{3+} ions into the La^{3+} sublattice (isovalent doping) leads to the expansion of the crystal lattice (Table 1). An increase in the size of the unit cell is observed during doping despite the close ionic radii of trivalent metals Pr^{3+} and La^{3+} ($r_{La^{3+}} = 1.216$ Å, $r_{Pr^{3+}} = 1.179$ Å [64]). The presence of ions with different electronegativity ($\chi_{La} = 1.10$, $\chi_{Pr} = 1.13$ [65]) could be the cause of the changes in the local structure and in the interatomic distances due to the additional repulsion effects. A similar effect was observed for another doped composition based on $BaLaInO_4$ [59,60], and the presence of ions with different electronegativity in the same sublattice can be considered as the reason of the changes in the crystal lattice size.

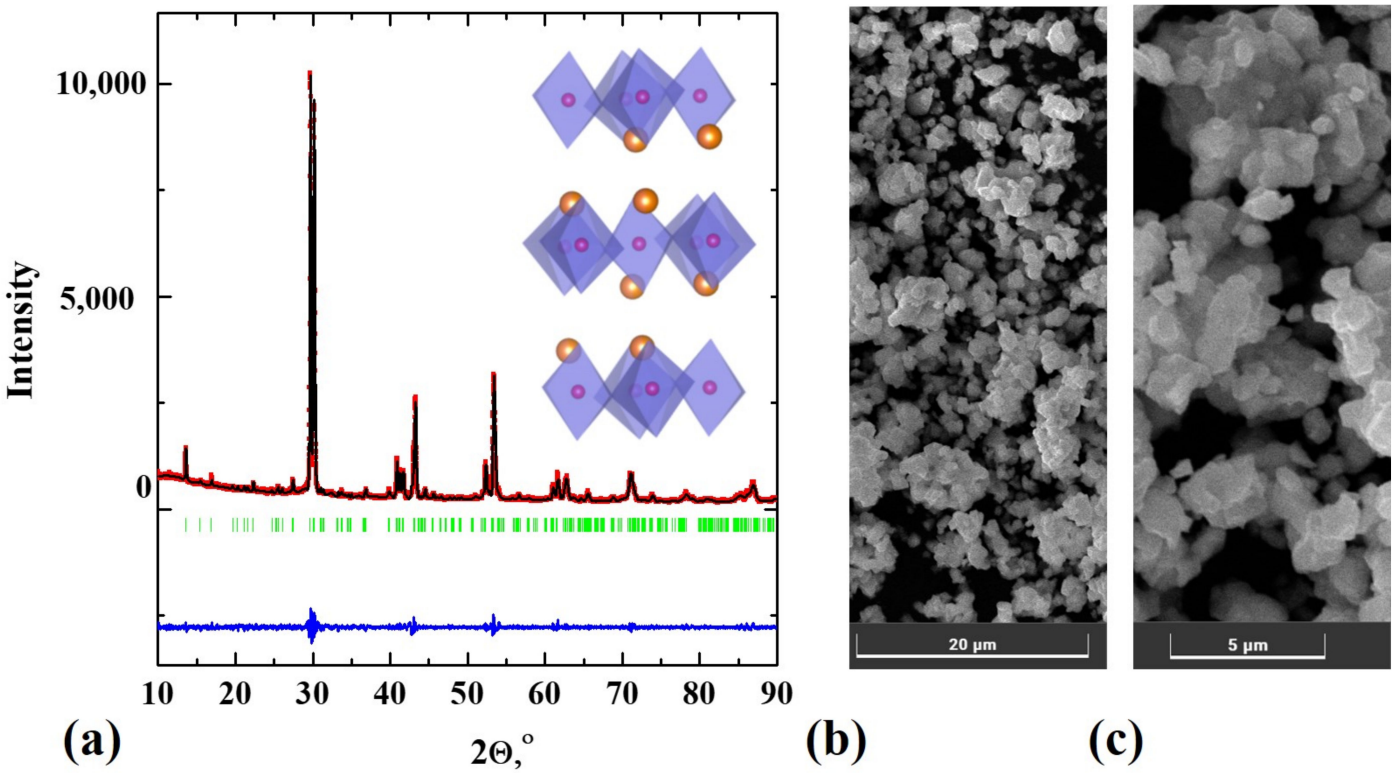

Figure 1. The results of the XRD—(**a**) (R_p = 2.11, R_{wp} = 2.25, χ^2 = 1.32) and SEM-investigations (**b**,**c**) for the composition $BaLa_{0.9}Pr_{0.1}InO_4$.

Table 1. The geometric characteristics of the crystal lattice for the compositions $BaLa_{0.9}Pr_{0.1}InO_4$ and $BaLaInO_4$.

Composition	*a*, Å	*b*, Å	*c*, Å	V, (Å^3)
$BaLa_{0.9}Pr_{0.1}InO_4$	12.968 (1)	5.911 (9)	5.917 (9)	453.17 (7)
$BaLaInO_4$ [56]	12.932 (3)	5.906 (0)	5.894 (2)	450.19 (5)

The morphology of the obtained sample was checked using scanning electron microscopy. Composition $BaLa_{0.9}Pr_{0.1}InO_4$ consists of grains (~3–5 µm) agglomerated in the particles with the size ~10 µm (Figure 1b,c). The elemental composition was proved via EDS analysis. The average element ratios for $BaLa_{0.9}Pr_{0.1}InO_4$ composition are presented in Table 2. The good agreement between theoretical and experimental values was confirmed.

Table 2. The results of the energy-dispersive analysis for the composition $BaLa_{0.9}Pr_{0.1}InO_4$ (theoretical values in atomic % are provided in the brackets).

Metal	Barium	Lanthanum	Praseodymium	Indium
Content	33.4	29.9	3.2	33.5
	(33.3)	(30.0)	(3.3)	(33.4)

The amount of water uptake was measured via thermogravimetry (TG) coupled with the differential scanning calorimetry (DSC) method. The results are presented in Figure 2. As we can see, the initially hydrated composition loses mass due to water release that was confirmed by MS-results. No other volatile components were detected. The main mass loss happens at ~ 200–400 °C, which is confirmed by the signal on the DSC-curve (green line in Figure 2). The dissociative water intercalation into the crystal structure of layered

perovskites is possible due to the placement of hydroxyl groups in the rock salt space of the layered framework [62]:

$$H_2O + O_o^x \Leftrightarrow (OH)_o^{\bullet} + (OH)_i^{'} \quad (1)$$

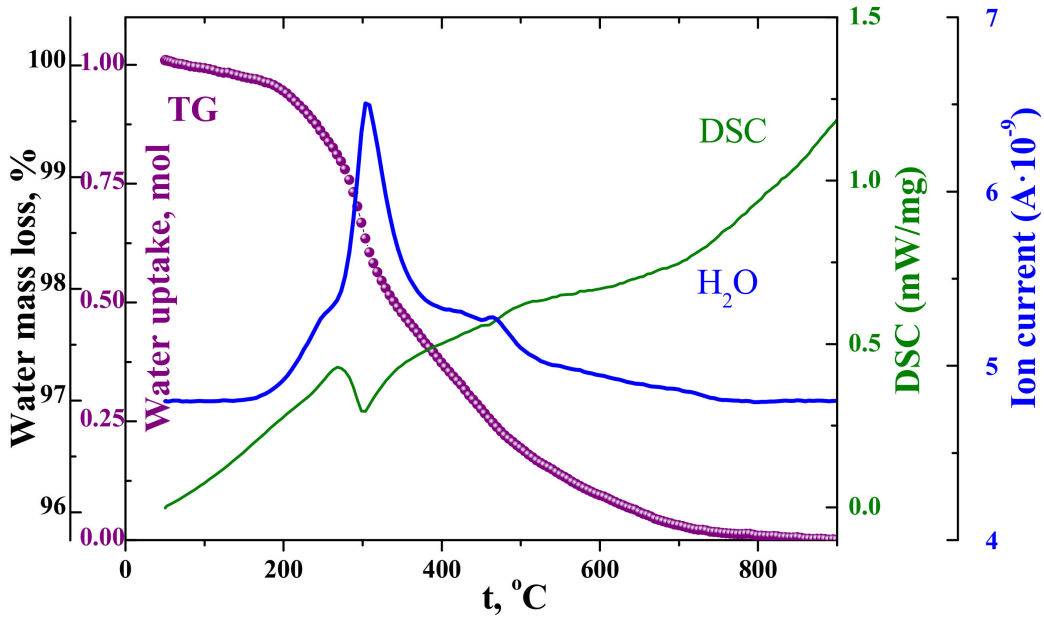

Figure 2. The TG, DSC and MS results for the composition $BaLa_{0.9}Pr_{0.1}InO_4$.

Consequently, the increasing of the crystal lattice size should lead to the increasing of the water uptake [62]. As we can see, the water uptake for the Pr-doped composition is about 1 mol water per formula unit (Figure 2), which is bigger than 0.62 mol registered for undoped $BaLaInO_4$ composition [62]. In other words, a good correlation between the changes of the geometric characteristics of the unit cell and water uptake is observed.

The electrotransport properties of the Pr-doped composition were investigated via the impedance spectroscopy method. Nyquist plots under dry and wet air at 400 °C are presented in Figure 3a as an example of collected data. The calculation of conductivity values was made using the resistance value obtained by extrapolating the high-frequency semicircle to the abscissa axis (capacitance ~10^{-12} F/cm). The effect of variation in oxygen partial pressure to the conductivity values is presented in Figure 3b. As we can see, the electrical conductivity is mixed hole ionic at dry oxidizing conditions. The share of oxygen ionic transport does not change at the temperature variation, and it is around 25%, which is comparable with the value (20%) for undoped $BaLaInO_4$ composition [56]. We can suggest that the dopant concentration of 0.1 mol is not enough to have a meaningful impact on the conductivity nature. At the same time, the nature of dopant is also a possible reason for the absence of significant changes in the nature of conductivity. However, a significant increase in the conductivity values (~1.5 orders of magnitude) during doping is observed (Figure 3c,d). The most probable reason for the increase in the mobility of oxygen ions is due to the increase in the size of the crystal lattice and space for ionic transport. It should be noted that the conductivity values from the electrolytic area (oxygen ionic conductivity, $pO_2 < 10^{-5}$) do correlate well with the conductivity values obtained at the Ar atmosphere. This allows us to consider the values obtained in argon as ionic conductivity values.

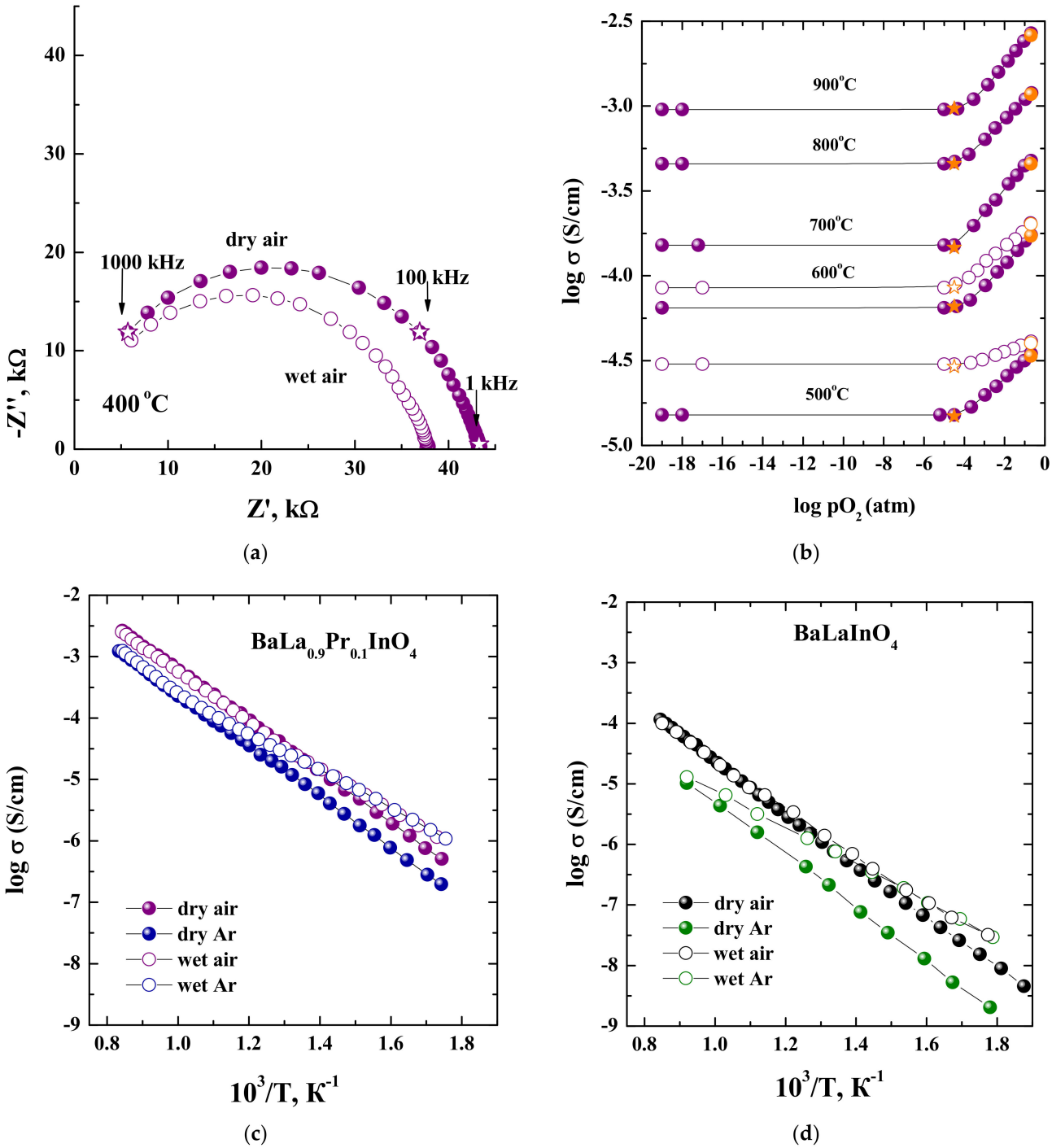

Figure 3. The Nyquist plots for the composition $BaLa_{0.9}Pr_{0.1}InO_4$ obtained under dry and wet air at 400 °C (**a**), the dependencies σ – pO_2 for the composition $BaLa_{0.9}Pr_{0.1}InO_4$ (violet symbols) at dry (closed symbols) and wet (open symbols) atmospheres (**b**), the dependencies σ –1000/T for the compositions $BaLa_{0.9}Pr_{0.1}InO_4$ (**c**) and $BaLaInO_4$ [56] (**d**).

The humidity of the atmosphere affects the conductivity values below 600 °C. The proton concentration increases with temperature decreases. This is because of the increase of the conductivity under wet conditions in comparison with dry conditions (Figure 3b,c). The proton conductivity was calculated as the difference between conductivity values obtained under *wet Ar* and *dry Ar*:

$$\sigma_{H^+} = \sigma_{wet\ Ar} - \sigma_{dry\ Ar} = \sigma_{wet}^{ion} - \sigma_{dry}^{ion} \quad (2)$$

and its temperature dependencies are shown in Figure 4a. As we can see, the protonic conductivity for the Pr-doped composition is higher than the undoped sample by ~1.5 orders of magnitude. This increase is due to the increase in both the proton concentration and proton mobility (Figure 4b). The proton conductivity value for doped $BaLa_{0.9}Pr_{0.1}InO_4$ composition is 5.0 × 10^{-6} S/cm (T = 400 °C) in comparison with 2.7 ×·10^{-7} S/cm for $BaLaInO_4$ composition that is 18 times greater. It can be suggested that the change in the dopant concentration and dopant nature can lead to significant changes in the nature of electrical conductivity.

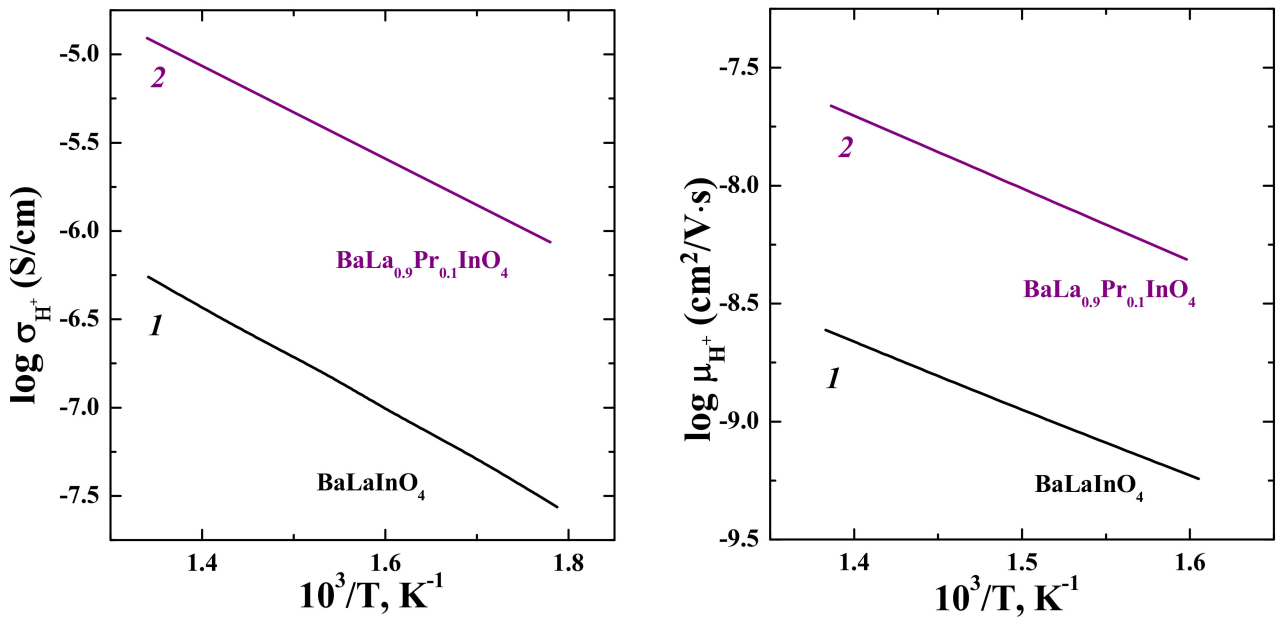

(**a**) (**b**)

Figure 4. The dependencies of conductivity (**a**) and mobility (**b**) of protons vs. temperature for the compositions $BaLa_{0.9}Pr_{0.1}InO_4$ and BaLaInO4 [56].

4. Conclusions

The layered perovskite $BaLa_{0.9}Pr_{0.1}InO_4$ was obtained and investigated as a protonic conductor for the first time. The possibility of proton transport is shown. It was proved that isovalent doping $Pr^{3+} \rightarrow La^{3+}$ leads to an increase in the crystal lattice size, proton concentration and proton mobility. The proton conductivity value for the doped $BaLa_{0.9}Pr_{0.1}InO_4$ composition is 5.0 ×·10^{-6} S/cm (T = 400 °C), in comparison with the 2.7·× 10^{-7} S/cm for $BaLaInO_4$ composition that is 18 times greater. Further research for a dopant capable of a significant change in its electrical conductivity nature is relevant. Layered perovskites based on $BaLaInO_4$ are promising materials for application in proton conducting
electrochemical devices.

Author Contributions: Conceptualization, I.A. and N.T.; methodology, I.A. and N.T.; investigation, A.B.; data curation, N.T. and A.B.; writing—original draft preparation, N.T.; writing—review and editing, N.T. and I.A. All authors have read and agreed to the published version of the manuscript.

Funding: This research was supported by the Russian Science Foundation (grant no 22-79-10003).

Institutional Review Board Statement: Not applicable.

Informed Consent Statement: Not applicable.

Data Availability Statement: Not applicable.

Conflicts of Interest: The authors declare no conflict of interest.

References

1. Punj, P.; Singh, J.; Singh, K. Ceramic biomaterials: Properties, state of the art and future prospectives. *Ceram. Int.* **2021**, *47*, 28059–28074. [CrossRef]
2. Koons, G.L.; Diba, M.; Mikos, A.G. Materials design for bone-tissue engineering. *Nat. Rev. Mater.* **2020**, *5*, 584–603. [CrossRef]
3. Jodati, H.; Yilmaz, B.; Evis, Z. Calcium zirconium silicate (baghdadite) ceramic as a biomaterial. *Ceram. Int.* **2022**, *46*, 21902–21909. [CrossRef]
4. Weng, W.; Wu, W.; Hou, M.; Liu, T.; Wang, T.; Yang, H. Review of zirconia-based biomimetic scaffolds for bone tissue engineering. *J. Mater. Sci.* **2022**, *56*, 8309–8333. [CrossRef]
5. Bunpetch, V.; Zhang, X.; Li, T.; Lin, J.; Maswikiti, E.P.; Wu, Y.; Cai, D.; Li, J.; Zhang, S.; Wu, C.; et al. Silicate-based bioceramic scaffolds for dual-lineage regeneration of osteochondral defect. *Biomaterials* **2019**, *192*, 323–333. [CrossRef]
6. Tarasova, N.; Galisheva, A.; Belova, K.; Mushnikova, A.; Volokitina, E. Ceramic materials based on lanthanum zirconate for the bone augmentation purposes: Materials science approach. *Chim. Techno Acta* **2022**, *9*, 20229209. [CrossRef]
7. Zvonareva, I.; Fu, X.-Z.; Medvedev, D.; Shao, Z. Electrochemistry and energy conversion features of protonic ceramic cells with mixed ionic-electronic electrolytes. *Energy Environ. Sci.* **2022**, *15*, 439–465. [CrossRef]
8. Shim, J.H. Ceramics breakthrough. *Nat. Energy* **2018**, *3*, 168–169. [CrossRef]
9. Bello, I.T.; Zhai, S.; He, Q.; Cheng, C.; Dai, Y.; Chen, B.; Zhang, Y.; Ni, M. Materials development and prospective for protonic ceramic fuel cells. *Int. J. Energy Res.* **2021**, *46*, 2212–2240. [CrossRef]
10. Zhang, W.; Hu, Y.H. Progress in proton-conducting oxides as electrolytes for low-temperature solid oxide fuel cells: From materials to devices. *Energy Sci. Eng.* **2021**, *9*, 984–1011. [CrossRef]
11. Meng, Y.; Gao, J.; Zhao, Z.; Amoroso, J.; Tong, J.; Brinkman, K.S. Review: Recent progress in low-temperature proton-conducting ceramics. *J. Mater. Sci.* **2019**, *54*, 9291–9312. [CrossRef]
12. Medvedev, D. Trends in research and development of protonic ceramic electrolysis cells. *Int. J. Hydrogen Energy* **2019**, *44*, 26711–26740. [CrossRef]
13. Malerba, D. Poverty-energy-emissions pathways: Recent trends and future sustainable development goals. *Int. J. Sustain. Energy Dev.* **2019**, *49*, 109–124. [CrossRef]
14. Buonomano, A.; Barone, G.; Forzano, C. Advanced energy technologies, methods, and policies to support the sustainable development of energy, water and environment systems. *Energy Rep.* **2022**, *8*, 4844–4853. [CrossRef]
15. Chu, S.; Majumdar, A. Opportunities and challenges for a sustainable energy future. *Nature* **2012**, *48*, 294–303. [CrossRef] [PubMed]
16. Østergaard, P.A.; Duic, N.; Noorollahi, Y.; Mikulcic, H.; Kalogirou, S. Sustainable development using renewable energy technology. *Renew. Energy* **2020**, *146*, 2430–2437. [CrossRef]
17. Olabi, A.G.; Abdelkareem, M.A. Renewable energy and climate change. *Renew. Sustain. Energy Rev.* **2022**, *158*, 112111. [CrossRef]
18. Corvalan, C.; Prats, E.V.; Sena, A.; Campbell-Lendrum, D.; Karliner, J.; Risso, A.; Wilburn, S.; Slotterback, S.; Rathi, M.; Stringer, R.; et al. Towards climate resilient and environmentally sustainable health care facilities. *Int. J. Environ. Res. Public Health* **2020**, *17*, 8849. [CrossRef]
19. Watts, N.; Amann, M.; Arnell, N.; Ayeb-Karlsson, S.; Beagley, J.; Belesova, K.; Boykoff, M.; Byass, P.; Cai, W.; Campbell-Lendrum, D.; et al. The 2020 report of the Lancet countdown on health and climate change: Responding to converging crises. *Lancet* **2021**, *397*, 129–170. [CrossRef]
20. Kats, G.H. Slowing global warming and sustaining development: The promise of energy efficiency. *Energy Policy* **1990**, *18*, 25–33. [CrossRef]
21. Afroze, S.; Reza, M.S.; Cheok, Q.; Taweekun, J.; Azad, A.K. Solid oxide fuel cell (SOFC); A new approach of energy generation during the pandemic COVID-19. *Int. J. Integr. Eng.* **2020**, *12*, 245–256. [CrossRef]
22. Stambouli, A.B.; Traversa, E. Solid oxide fuel cells (SOFCs): A review of an environmentally clean and efficient source of energy. *Renew. Sustain. Energy Rev.* **2002**, *6*, 433–455. [CrossRef]
23. Afroze, S.; Reza, M.S.; Cheok, Q.; Islam, S.N.; Abdalla, A.M.; Taweekun, J.; Azad, A.K.; Khalilpoor, N.; Issakhov, A. Advanced applications of fuel cells during the COVID-19 Pandemic. *Int. J. Chem. Eng.* **2021**, *2021*, 5539048. [CrossRef]
24. Dincer, I. Renewable energy and sustainable development: A crucial review. *Renew. Sustain. Energy Rev.* **2000**, *4*, 157–175. [CrossRef]
25. Panwar, N.L.; Kaushik, S.C.; Kothari, S. Role of renewable energy sources in environmental protection: A review. *Renew. Sustain. Energy Rev.* **2011**, *15*, 1513–1524. [CrossRef]
26. Dincer, I.; Rosen, M.A. Sustainability aspects of hydrogen and fuel cell systems. *Int. J. Sustain. Energy Dev.* **2011**, *15*, 137–146. [CrossRef]
27. Branco, H.; Castro, R.; Lopes, A.S. Battery energy storage systems as a way to integrate renewable energy in small isolated power systems. *Int. J. Sustain. Energy Dev.* **2018**, *43*, 90–99. [CrossRef]
28. International Energy Agency. *The Future of Hydrogen: Seizing Today's Opportunities*; OECD: Paris, France, 2019. [CrossRef]
29. Abe, J.O.; Popoola, A.P.I.; Ajenifuja, E.; Popoola, O.M. Hydrogen energy, economy and storage: Review and recommendation. *Int. J. Hydrogen Energy* **2019**, *44*, 15072–15086. [CrossRef]
30. Dawood, F.; Anda, M.; Shafiullah, G.M. Hydrogen production for energy: An overview. *Int. J. Hydrogen Energy* **2019**, *45*, 3847–3869. [CrossRef]

31. Easily, R.R.; Chi, Y.; Ibrahiem, D.M.; Chen, Y. Hydrogen strategy in decarbonization era: Egypt as a case study. *Int. J. Hydrogen Energy* **2022**, *47*, 18629–18647. [CrossRef]
32. Arsad, A.Z.; Hannan, M.A.; Al-Shetwi, A.Q.; Mansur, M.; Muttaqi, K.M.; Dong, Z.Y.; Blaabjerg, F. Hydrogen energy storage integrated hybrid renewable energy systems: A review analysis for future research directions. *Int. J. Hydrogen Energy* **2022**, *47*, 17285–17312. [CrossRef]
33. Scovell, M.D. Explaining hydrogen energy technology acceptance: A critical review. *Int. J. Hydrogen Energy* **2022**, *47*, 10441–10459. [CrossRef]
34. Abdalla, A.M.; Hossain, S.; Nisfindy, O.B.; Azad, A.T.; Dawood, M.; Azad, A.K. Hydrogen production, storage, transportation and key challenges with applications: A review. *Energy Convers. Manag.* **2018**, *165*, 602–627. [CrossRef]
35. Hossain, S.; Abdalla, A.M.; Jamain, S.N.B.; Zaini, J.H.; Azad, A.K. A review on proton conducting electrolytes for clean energy and intermediate temperature-solid oxide fuel cells. *Renew. Sustain. Energy Rev.* **2017**, *79*, 750–764. [CrossRef]
36. Kasyanova, A.; Zvonareva, I.; Bi, L.; Medvedev, D.; Shao, Z. Electrolyte materials for protonic ceramic electrochemical cells: Main limitations and potential solutions. *Mater. Rep. Energy* **2022**, *2*, 100158. [CrossRef]
37. Kim, J.; Sengodan, S.; Kim, S.; Kwon, O.; Bu, Y.; Kim, G. Proton conducting oxides: A review of materials and applications for renewable energy conversion and storage. *Renew. Sustain. Energy Rev.* **2019**, *109*, 606–618. [CrossRef]
38. Chiara, A.; Giannici, F.; Pipitone, C.; Longo, A.; Aliotta, C.; Gambino, M.; Martorana, A. Solid-solid interfaces in protonic ceramic devices: A critical review. *ACS Appl. Mater. Interfaces* **2020**, *12*, 55537–55553. [CrossRef] [PubMed]
39. Cao, J.; Ji, Y.; Shao, Z. New insights into the proton-conducting solid oxide fuel cells. *J. Chin. Ceram. Soc.* **2021**, *49*, 83–92. [CrossRef]
40. Bello, I.T.; Zhai, S.; Zhao, S.; Li, Z.; Yu, N.; Ni, M. Scientometric review of proton-conducting solid oxide fuel cells. *Int. J. Hydrogen Energy* **2021**, *46*, 37406–37428. [CrossRef]
41. Colomban, P. Proton conductors and their applications: A tentative historical overview of the early researches. *Solid State Ion.* **2019**, *334*, 125–144. [CrossRef]
42. Syafkeena, M.A.N.; Zainor, M.L.; Hassan, O.H.; Baharuddin, N.A.; Othman, M.H.D.; Tseng, C.-J.; Osman, N. Review on the preparation of electrolyte thin films based on cerate-zirconate oxides for electrochemical analysis of anode-supported proton ceramic fuel cells. *J. Alloys Compd.* **2022**, *918*, 165434. [CrossRef]
43. Rasaki, S.A.; Liu, C.; Lao, C. A review of current performance of rare earth metal-doped barium zirconate perovskite: The promising electrode and electrolyte material for the protonic ceramic fuel cells. *Prog. Solid State Chem.* **2021**, *63*, 100325. [CrossRef]
44. Fujii, K.; Shiraiwa, M.; Esaki, Y.; Yashima, M.; Kim, S.J.; Lee, S. Improved oxide-ion conductivity of $NdBaInO_4$ by Sr doping. *J. Mater. Chem. A* **2015**, *3*, 11985–11990. [CrossRef]
45. Ishihara, T.; Yan, Y.; Sakai, T.; Ida, S. Oxide ion conductivity in doped $NdBaInO_4$. *Solid State Ion.* **2016**, *288*, 262–265. [CrossRef]
46. Yang, X.; Liu, S.; Lu, F.; Xu, J.; Kuang, X. Acceptor doping and oxygen vacancy migration in layered perovskite $NdBaInO_4$- based mixed conductors. *J. Phys. Chem. C* **2016**, *12*, 6416–6426. [CrossRef]
47. Fujii, K.; Yashima, M. Discovery and development of $BaNdInO_4$–A brief review. *J. Ceram. Soc.* **2018**, *126*, 852–859. [CrossRef]
48. Zhou, Y.; Shiraiwa, M.; Nagao, M.; Fujii, K.; Tanaka, I.; Yashima, M.; Baque, L.; Basbus, J.F.; Mogni, L.V.; Skinner, S.J. Protonic conduction in the $BaNdInO_4$ structure achieved by acceptor doping. *Chem. Mater.* **2021**, *33*, 2139–2146. [CrossRef]
49. Shiraiwa, M.; Kido, T.; Fujii, K.; Yashima, M. High-temperature proton conductors based on the (110) layered perovskite $BaNdScO_4$. *J. Mat. Chem. A* **2021**, *9*, 8607–8619. [CrossRef]
50. Kato, S.; Ogasawara, M.; Sugai, M.; Nakata, S. Synthesis and oxide ion conductivity of new layered perovskite $La_{1-x}Sr_{1+x}InO_{4-d}$. *Solid State Ion.* **2002**, *149*, 53–57. [CrossRef]
51. Troncoso, L.; Alonso, J.A.; Aguadero, A. Low activation energies for interstitial oxygen conduction in the layered perovskites $La_{1+x}Sr_{1-x}InO_{4+d}$. *J. Mater. Chem. A* **2015**, *3*, 17797–17803. [CrossRef]
52. Troncoso, L.; Alonso, J.A.; Fernández-Díaz, M.T.; Aguadero, A. Introduction of interstitial oxygen atoms in the layered perovskite $LaSrIn_{1-x}B_xO_{4+\delta}$ system (B = Zr, Ti). *Solid State Ion.* **2015**, *282*, 82–87. [CrossRef]
53. Troncoso, L.; Mariño, C.; Arce, M.D.; Alonso, J.A. Dual oxygen defects in layered $La_{1.2}Sr_{0.8-x}Ba_xInO_{4+d}$ (x = 0.2, 0.3) oxide-ion conductors: A neutron diffraction study. *Materials* **2019**, *12*, 1624. [CrossRef] [PubMed]
54. Troncoso, L.; Arce, M.D.; Fernández-Díaz, M.T.; Mogni, L.V.; Alonso, J.A. Water insertion and combined interstitial-vacancy oxygen conduction in the layered perovskites $La_{1.2}Sr_{0.8-x}Ba_xInO_{4+d}$. *New J. Chem.* **2019**, *43*, 6087–6094. [CrossRef]
55. Tarasova, N.; Animitsa, I.; Galisheva, A. Effect of acceptor and donor doping on the state of protons in block-layered structures based on $BaLaInO_4$. *Solid State Commun.* **2021**, *323*, 114093. [CrossRef]
56. Tarasova, N.; Galisheva, A.; Animitsa, I. Improvement of oxygen-ionic and protonic conductivity of $BaLaInO_4$ through Ti doping. *Ionics* **2020**, *26*, 5075–5088. [CrossRef]
57. Tarasova, N.; Galisheva, A.; Animitsa, I.; Korona, D.; Davletbaev, K. Novel proton-conducting layered perovskite based on $BaLaInO_4$ with two different cations in B-sublattice: Synthesis, hydration, ionic (O^{2+}, H^+) conductivity. *Int. J. Hydrogen Energy* **2022**, *47*, 18972–18982. [CrossRef]
58. Tarasova, N.; Galisheva, A.; Animitsa, I.; Anokhina, I.; Gilev, A.; Cheremisina, P. Novel mid-temperature $Y^{3+} \rightarrow In^{3+}$ doped proton conductors based on the layered perovskite $BaLaInO_4$. *Ceram. Int.* **2022**, *48*, 15677–15685. [CrossRef]
59. Tarasova, N.; Bedarkova, A.; Animitsa, I. Proton transport in the gadolinium-doped layered perovskite $BaLaInO_4$. *Materials* **2022**, *15*, 7351. [CrossRef]

60. Tarasova, N.; Bedarkova, A. Advanced proton-conducting ceramics based on layered perovskite $BaLaInO_4$ for energy conversion technologies and devices. *Materials* **2022**, *15*, 6841. [CrossRef]
61. Tarasova, N.; Animitsa, I.; Galisheva, A.; Medvedev, D. Layered and hexagonal perovskites as novel classes of proton-conducting solid electrolytes: A focus review. *Electrochem. Mater. Technol.* **2022**, *1*, 20221004. [CrossRef]
62. Tarasova, N.; Animitsa, I. Materials $A^{II}LnInO_4$ with Ruddlesden-Popper structure for electrochemical applications: Relationship between ion (oxygen-ion, proton) conductivity, water uptake and structural changes. *Materials* **2022**, *15*, 114. [CrossRef] [PubMed]
63. Tarasova, N.; Galisheva, A. Phosphorus-doped protonic conductors based on $BaLa_nIn_nO_{3n+1}$ (n = 1, 2): Applying oxyanion doping strategy to the layered perovskite structures. *Chim. Techno Acta* **2022**, *9*, 20229405. [CrossRef]
64. Shannon, R.D. Revised effective ionic radii and systematic studies of interatomic distances in halides and chalcogenides. *Acta Cryst.* **1976**, *A32*, 751–767. [CrossRef]
65. Allred, A.L. Electronegativity values from thermochemical data. *J. Inorg. Nucl. Chem.* **1961**, *17*, 215–221. [CrossRef]